4 Radar Environment

4.1 Atmospheric Losses

The atmosphere, also called the troposphere, produces losses in radar signal propagation due to atmospheric attenuation, and to beam spreading.

Atmospheric attenuation. This loss is caused by molecular absorption by oxygen and water vapor in the atmosphere. The loss increases gradually with frequency in the microwave-frequency region, and has resonant peaks at 22.3 GHz due to water vapor and at 60 GHz due to oxygen. The attenuation decreases with altitude, and usually can be neglected above 10 km. For surface radars, the attenuation decreases with increasing elevation angle, and can usually be neglected at elevation angles above 10 degrees.

Atmospheric loss increases exponentially with path length, l, and can be characterized by a two-way loss in dB per km, a_A (Fig. 4.1). For paths where a_A remains constant, the total loss, L_A, in dB is:

$$L_A(\text{in dB}) = a_A\, l \tag{4.1}$$

The loss power ratio is:

$$L_A\ (\text{power ratio}) = 10^{\frac{a_A l}{10}} \tag{4.2}$$

For signal paths where a_A varies, the attenuation is found by integrating along the signal path. Values for surface radars are given as functions of range and elevation angle for UHF, L, S, C, and X bands in Figs. 4.2 through 4.6 [27].

Lens loss. At low elevation angles the difference in atmospheric refraction (Sec. 4.3), at the top and bottom of the beam increases the elevation beamwidth, reducing the gain. This is characterized as the lens loss. The loss is independent of frequency, increases with range, and decreases with increasing elevation angle. It usually can be neglected at elevation angles greater than 5 degrees. Values of lens loss for surface radars are given as a function of range and elevation angle in Fig. 4.7 [28, Ch, 15]. Values for other radar altitudes can be found in [28, Ch. 15].

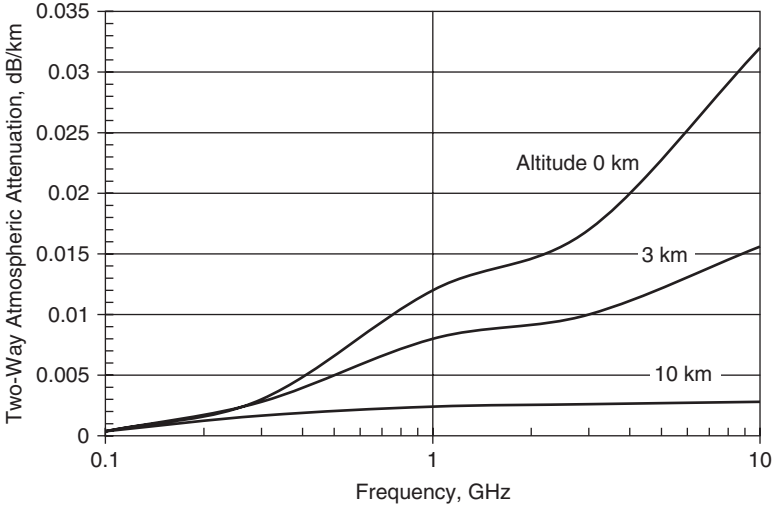

Fig. 4.1 Atmospheric attenuation coefficient, a_A, vs. frequency and elevation angle (made using the custom radar functions in [5])

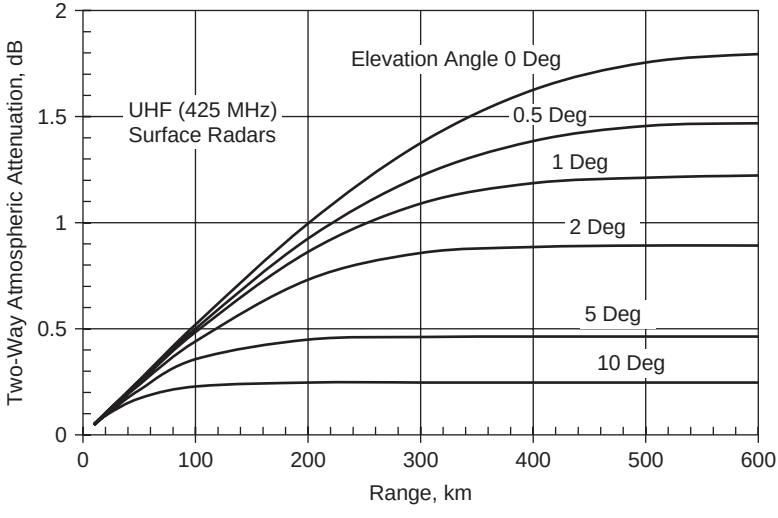

Fig. 4.2 Atmospheric attenuation at UHF vs. range and elevation angle for surface radars (made using the custom radar functions in [5])

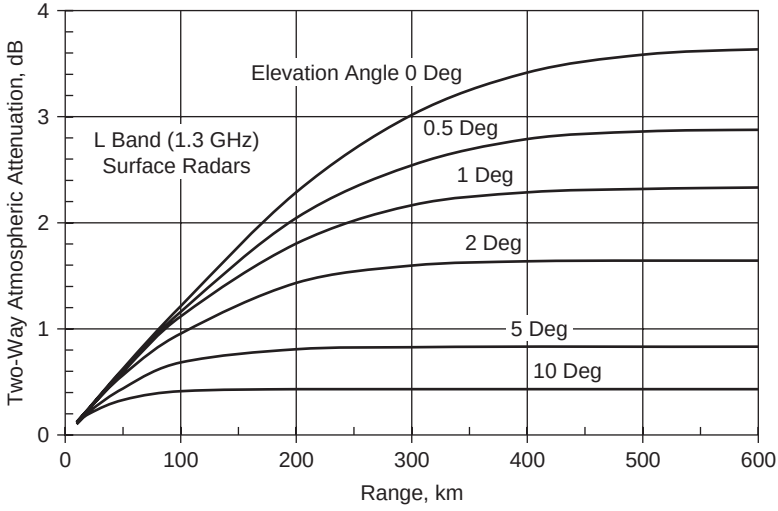

Fig. 4.3 Atmospheric attenuation at L band vs. range and elevation angle for surface radars (made using the custom radar functions in [5])

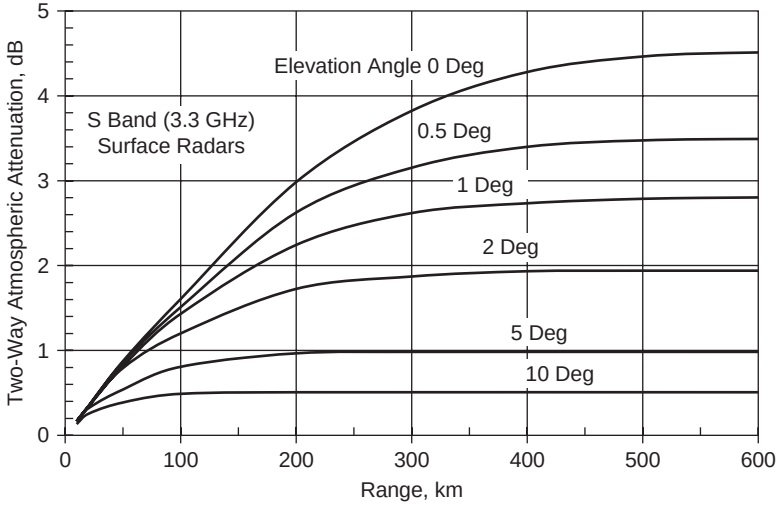

Fig. 4.4 Atmospheric attenuation at S band vs. range and elevation angle for surface radars (made using the custom radar functions in [5])

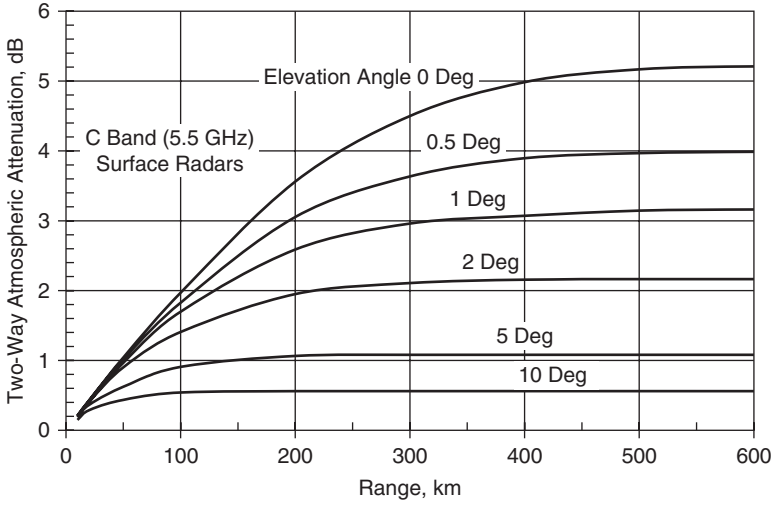

Fig. 4.5 Atmospheric attenuation at C band vs. range and elevation angle for surface radars (made using the custom radar functions in [5])

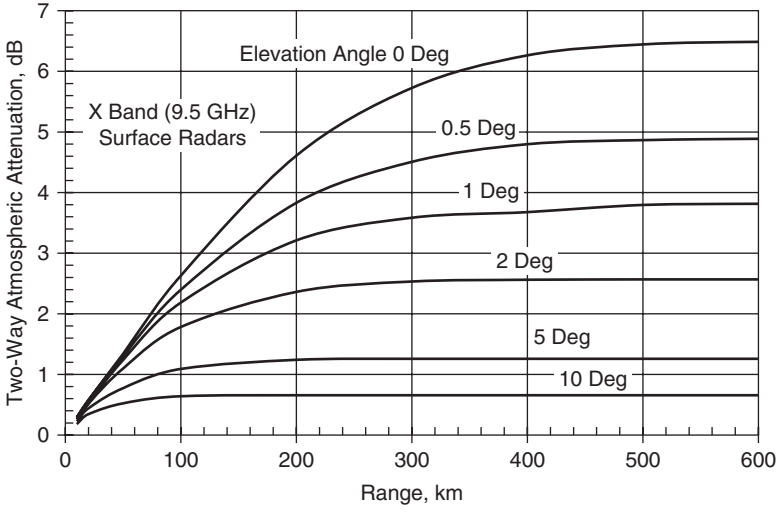

Fig. 4.6 Atmospheric attenuation at X band vs. range and elevation angle for surface radars (made using the custom radar functions in [5])

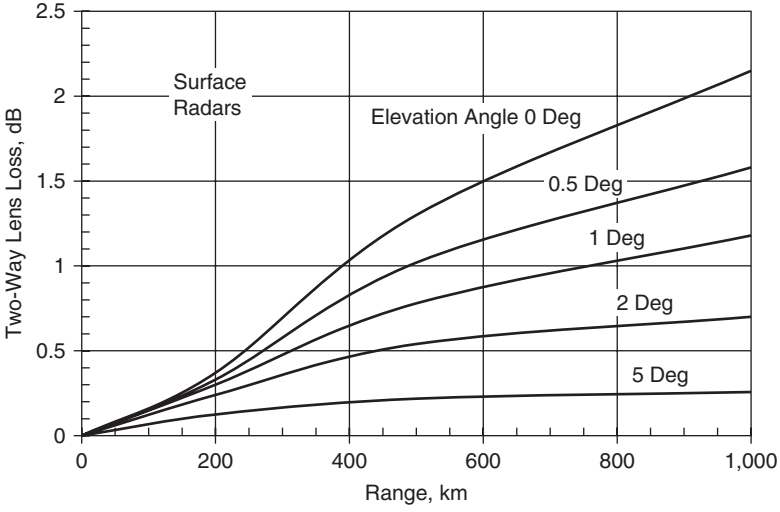

Fig. 4.7 Lens loss vs. range and elevation angle for surface radars (made using the custom radar functions in [5])

The lens loss from Fig. 4.7 should be added to the atmospheric attenuation from Figs. 4.2 through 4.6 to get the total atmospheric losses.

4.2 Rain Loss

Rain causes signal attenuation for signal paths that pass through the rainfall. The attenuation increases significantly with frequency, and can usually be neglected at frequencies below 1 GHz. Rain loss increases exponentially with path length, l, and can be characterized by a two-way loss in dB per km, a_R (Fig. 4.8), [29, Ch. 1]. For paths where a_R remains constant, the total loss, L_R, in dB is:

$$L_R(\text{in dB}) = a_R\, l \tag{4.3}$$

The loss power ratio is:

$$L_R \text{ (power ratio)} = 10^{\frac{a_R l}{10}} \tag{4.4}$$

The signal attenuation is found by integrating the attenuation along the signal path. Since only liquid rain produces significant attenuation, only the portion of signal paths below the zero-degree isotherm, (about 3 km altitude at mid latitudes), will experience rain loss. Also, rainfall is not uniform over extended areas. High rainfall rates are usually confined to relatively small areas, typically 10 km or less. Thus, Eqs. 4.3 and 4.4

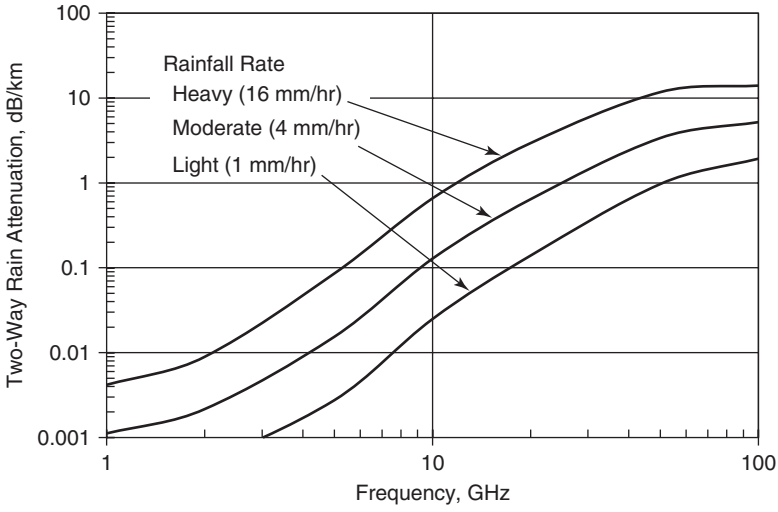

Fig. 4.8 Rain attenuation coefficient, a_R, vs. frequency (made using the custom radar functions in [5])

must be used with care. A model for predicting probable path loss from rainfall was developed by Crane [29, Ch. 4].

4.3 Atmospheric Refraction

Refraction or bending of the radar-signal propagation path in the atmosphere (also called the troposphere), is caused by small variations of the propagation velocity with altitude due to variations in pressure, temperature, and water vapor content. The refractive index, n, is the ratio of the propagation velocity to that in a vacuum. It normally decreases with increasing altitude, causing a downward bending and lengthening of the propagation path.

The atmospheric refractivity, N, is:

$$N = 10^6 (n - 1) \tag{4.5}$$

It normally decreases approximately exponentially with increasing altitude. The refractivity at the earth's surface has a standard value of 313, and can vary over a range of about $\pm 10\%$.

Measurement errors. Atmospheric refraction produces errors in radar measurements of range and elevation angle. These errors decrease with increasing elevation angle, and are independent of frequency for frequencies below about 20 GHz (Figs. 4.9 and 4.10), [10, App. D]).

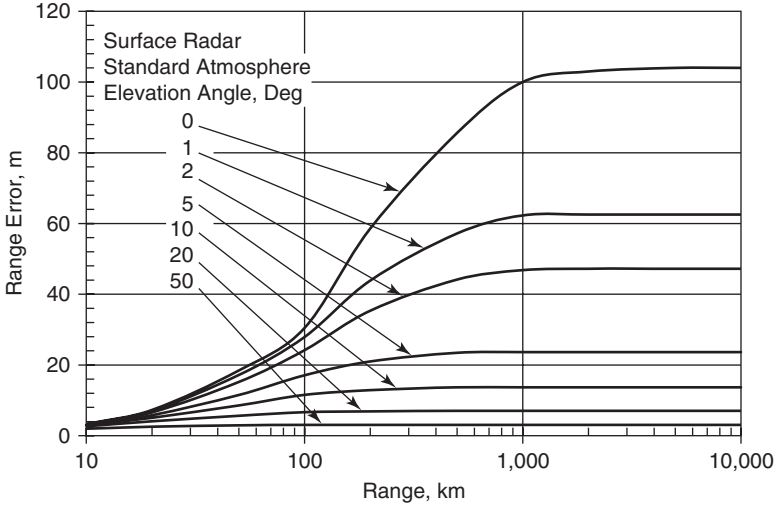

Fig. 4.9 Range-measurement error vs. range and elevation angle for a surface radar and standard atmosphere (made using the custom radar functions in [5])

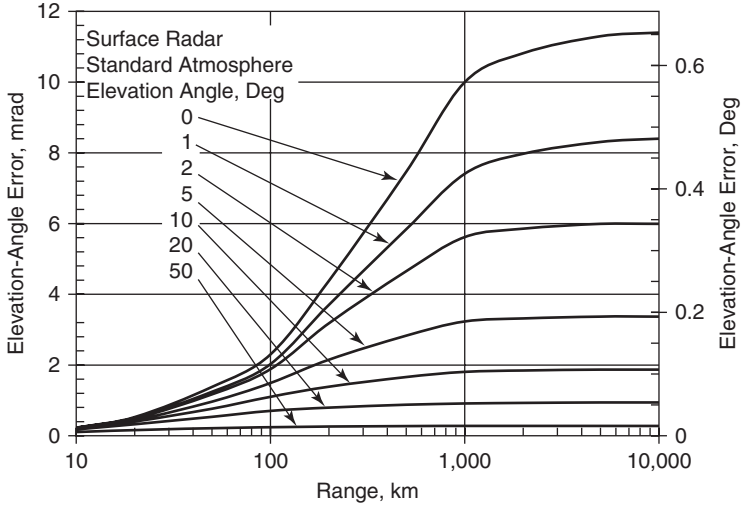

Fig. 4.10 Elevation-angle-measurement error vs. range and elevation angle for a surface radar and standard atmosphere (made using the custom radar functions in [5])

The atmospheric measurement errors can be corrected to an accuracy of about 15% of their magnitude by using data for a standard atmosphere, such as in Figs. 4.9 and 4.10. If the refractivity at the radar is measured, the accuracy of the correction improves to about 5% [6, Ch. 6]. These errors normally remain fixed during an observation, and are treated as bias errors when determining overall measurement accuracy (Sec. 3.5).

4/3 earth model. Atmospheric refraction paths are often modeled by assuming an earth radius that is 4/3 times the actual radius of 6,371 km, giving a value of 8,495 km. With this model, propagation paths within the atmosphere are approximately straight lines. This approximation is accurate for altitudes below 4 km, and is often used for altitudes up to 10 km with small error [5, Ch. 9]

Anomalous propagation (ducting). Atmospheric conditions can occur that produce refractivity above the earth's surface that decreases much more rapidly than in a standard atmosphere. This occurs most frequently over tropical ocean areas. The effect increases the refraction for surface radars, and can produce propagation around the earth's curvature, a phenomenon called surface ducting. This can allow detection of surface and low-altitude targets at ranges much greater than normally, and can also lead to unexpected second- and multiple-time-around returns (Sec. 1.3).

4.4 Terrain Masking and Multipath

Radar horizon range. Blocking of the radar line-of-sight (LOS), by terrain or the sea surface can limit the observation of low-altitude targets by surface or low-altitude radars. The radar horizon range, (the range from the radar to the point where the LOS is tangent to the earth or sea surface), is shown versus radar altitude above a smooth earth in Fig. 4.11.

For radar altitudes less than about 10 km, the horizon range, R_H, can be found using the 4/3 earth model (Sec. 4.3):

$$R_H = \left(h_R^2 + 2\, r_E\, h_R\right)^{1/2} \tag{4.6}$$

where h_R is the radar altitude above a smooth earth and r_E is the 4/3 earth radius, 8,495 km. The horizon range from the target to the LOS tangent point can also be found from Fig. 4.11 or Eq. 4.6, using the target altitude above a smooth earth.

Maximum range limitation. The sum of the radar horizon range and the target horizon range is the maximum range at which the target can be observed, given the radar and target altitudes and a smooth earth.

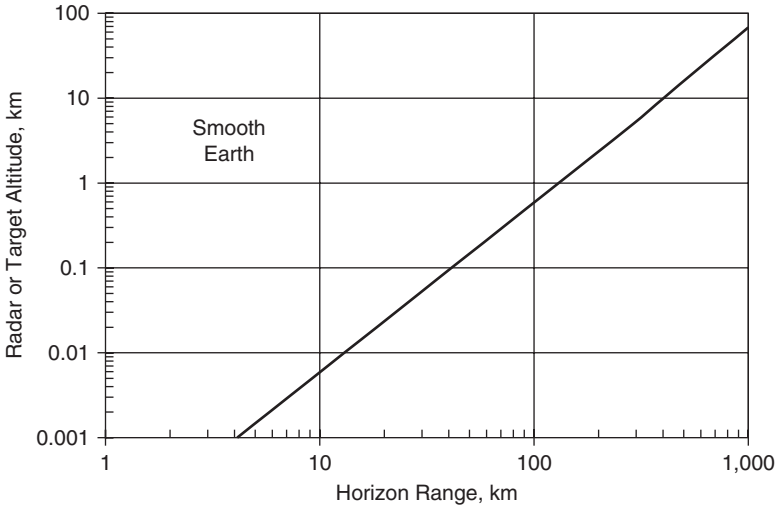

Fig. 4.11 Radar or target altitude vs. horizon range for a smooth earth

In many cases, radars are located at elevated sites to increase their horizon range. Conversely, hilly or mountainous terrain can reduce the radar or target horizon range. Also, it is often desirable to view targets at least a few degrees above the local horizon to avoid multipath propagation (see below), and to reduce atmospheric loss and refraction (Sec. 4.1 and 4.3). This will reduce the range at which low-altitude targets can be observed below that determined by the horizon ranges.

Multipath geometry. When the radar beam illuminates the terrain or sea surface between the radar and the target, as well as the target, a second, reflected, signal path between the radar and target is created. When the grazing angle (the angle between the earth's surface and the signal path), is small, the range difference between the direct signal path and the reflected signal path, δR, is small, and given approximately by:

$$\delta R \approx \frac{2\, h_R\, h_T}{R} \tag{4.7}$$

where h_R is the radar altitude, h_T is the target altitude, and R is the target direct-path range.

When δR is smaller than the radar range resolution, ΔR, the direct and reflected signals add coherently at the radar receiver, either increasing

or decreasing the received signal, depending on their relative phase. This effect is called multipath propagation. It can occur with:

- Rotating search radars that employ broad elevation-angle fan beams (Sec. 2.1).
- Pencil-beam antennas (Sec. 2.1), observing targets near the radar horizon.
- Airborne radars observing low-altitude targets with low signal-path grazing angles.
- Large structures (buildings, dams, etc.), that are illuminated by the radar beam and create a second signal path.

Multipath effects. With a flat, perfectly-reflecting surface, the received signal varies between zero and 16 times the signal level from the direct path alone. The resulting range for a given S/N varies between zero and twice the range when only the direct path is present due to the R^4 dependence on S/N. When the reflecting surface is not perfectly reflecting, or it is curved, the received signal peaks and nulls are less pronounced.

When the grazing angle is near zero, the received signal level and range are near their minimum, (zero for flat, perfectly-reflecting surfaces). As the elevation angle increases, a series of lobes are produced, separated in elevation angle by $\Delta\phi$, given by:

$$\Delta\phi = \frac{\lambda}{2\,h_R} \tag{4.8}$$

Multipath conditions can produce significant angle-measurement errors at low elevation angles [10, Ch. 5]

- For smooth reflecting surfaces, elevation-angle measurement errors are about half the elevation beamwidth for target elevations less than 0.8 of the elevation beamwidth. Smooth reflecting surfaces produce no azimuth-measurement errors.
- For rough reflecting surfaces and elevation angles less than the elevation beamwidth, elevation-angle measurement errors are typically 0.1 of the elevation beamwidth, and azimuth measurement errors are 0.1 to 0.2 of the azimuth beamwidth.

Measurement errors from multipath fluctuate slowly as the observation geometry changes, and should be treated as bias errors when combining them with other measurement errors (Sec. 3.5).

4.5 Radar Clutter

Radar returns from terrain or sea surface, or from rain, that interfere with the desired target signal are termed clutter. The interference level can be characterized by the ratio of the received signal power, S, to the clutter power, C. This signal-to-clutter ratio, S/C, depends on the target RCS, the amount of clutter illuminated, the clutter reflectivity and the effect of any clutter reduction techniques (Table 4.1). It is independent of radar sensitivity.

When the clutter signal has Gaussian probability distribution and is random from pulse-to-pulse, S/C can be combined with S/N:

$$\frac{S}{C+N} = \frac{1}{\frac{1}{S/C} + \frac{1}{S/N}} \tag{4.9}$$

This is often the case when many comparable scatterers are in the clutter resolution cell. Then, $S/(C+N)$ can be used in place of S/N in calculating radar detection and measurement performance (Sec. 3.3 and 3.5).

Surface clutter geometry. In most cases, the primary surface clutter that interferes with the target is from the same range-angle resolution cell as the target. (Sidelobe clutter can be significant for airborne radars using pulse-Doppler waveforms, and is discussed in Sec. 5.3.) The surface area of the clutter resolution cell, A_C, is usually given by:

$$A_C = \frac{R\,\theta_A\,\Delta R}{\cos\,\gamma} \qquad \left[\frac{\pi\,R\,\theta_E}{4\,\Delta R} \geq \tan\,\gamma\right] \tag{4.10}$$

TABLE 4.1 Characteristics of Surface and Rain Clutter

Clutter Source	**Terrain or Sea**	**Rain**
Clutter region	$A_C = \dfrac{R\,\theta_A\,\Delta R}{\cos\,\gamma}$	$V_C = \dfrac{\pi\,R^2\,\theta_A\,\theta_E\,\Delta R}{4}$
Clutter reflectivity	σ^0(m^2 RCS/m^2 surface)	η(m^2 RCS/m^3 volume)
Reflectivity factors	Depends on frequency, grazing angle γ, polarization, terrain, sea state	$\eta = \dfrac{6\times10^{-14}\,\text{rain rate (mm/hr)}^{1.6}}{\lambda^4}$
Clutter-reduction techniques (CR)	MTI Pulse-Doppler	Pulse-Doppler Polarization
Signal-to-clutter ratio	$\dfrac{S}{C} = \dfrac{\sigma\,\text{CRL}_{\text{BS}}}{\sigma^0\,A_C}\,(L_{BS}\approx1.5)$	$\dfrac{S}{C} = \dfrac{\sigma\,\text{CRL}_{\text{BS}}}{\eta\,V_C}\quad(L_{BS}\approx2.1)$

where R is the target range, θ_A is the azimuth beamwidth, θ_E is the elevation beamwidth, ΔR is the range resolution, and γ is the angle between the radar line-of-sight (LOS), and the surface, called the grazing angle.

For high grazing angles and large range resolution, the range extent of the clutter area may be determined by the elevation beamwidth, θ_E, rather than by the range resolution. Then A_C is:

$$A_C = \frac{\pi\, R^2\, \theta_A\, \theta_E}{4 \sin \gamma} \qquad \left[\frac{\pi\, R\, \theta_E}{4\, \Delta R} \leq \tan \gamma\right] \tag{4.11}$$

The clutter reflectivity is characterized by a parameter σ^0, which is dimensionless and is equal to the square meters of clutter RCS per square meter of surface area. The parameter σ^0 is usually significantly less than unity, and is often expressed by a negative dB value. (A larger reflectivity leads to a smaller negative dB value.) The clutter RCS in the resolution cell is given by:

$$\sigma_C = \frac{\sigma^0\, A_C}{L_{BS}} \tag{4.12}$$

Where L_{BS} is a beam-shape loss for the clutter, equal to about 1.5 (1.6 dB). The signal-to-clutter ratio is:

$$\frac{S}{C} = \frac{\sigma\, \mathrm{CRL_{BS}}}{\sigma^0\, A_C} \tag{4.13}$$

where CR is the clutter cancellation ratio, the improvement in S/C provided by clutter-reduction techniques such as those described later.

Surface reflectivity. The magnitude of the surface reflectivity, σ^0, is determined by several factors [30, 31, and 32]:

- Grazing angle. σ^0 varies approximately with the sine of grazing angle, γ, between grazing angles of a few degrees and about 60 deg. At the lower grazing angles, multipath interference produces lower reflectivity, while at high elevation angles specular returns result in higher values.
- Frequency. Sea clutter reflectivity is approximately proportional to frequency. For terrain, σ^0 generally increases with increasing radar frequency.
- Terrain type. σ^0 is generally larger for rougher terrain and for more pronounced vegetation. Large discrete returns, for example from buildings, produce non-Gaussian probability distributions.

- Sea state. σ^0 increases with sea state.
- Polarization. For smooth terrain and sea surface and low grazing angles, σ^0 is greater for vertical polarization than for horizontal polarization. For rough terrain and at high grazing angles, the difference in reflectivity between polarizations is small.

Representative plots of terrain and sea clutter reflectivity vs. grazing angle are shown in Figs. 4.12 and 4.13.

Surface clutter usually has a small velocity spread due to the motion of the clutter scatterers, producing a small Doppler-frequency spread for stationary radars:

- For terrain, the velocity spread ranges from near zero for rocky terrain, to about 0.33 m/s for wind-blown trees.
- For sea clutter, the velocity spread is approximately 0.125 times the wind velocity.
- Rotating search radars produce a velocity spread component equal to the velocity of the antenna edge.

Rain clutter. In most cases, the primary rain clutter that interferes with the target is from the same range-angle resolution cell as the target.

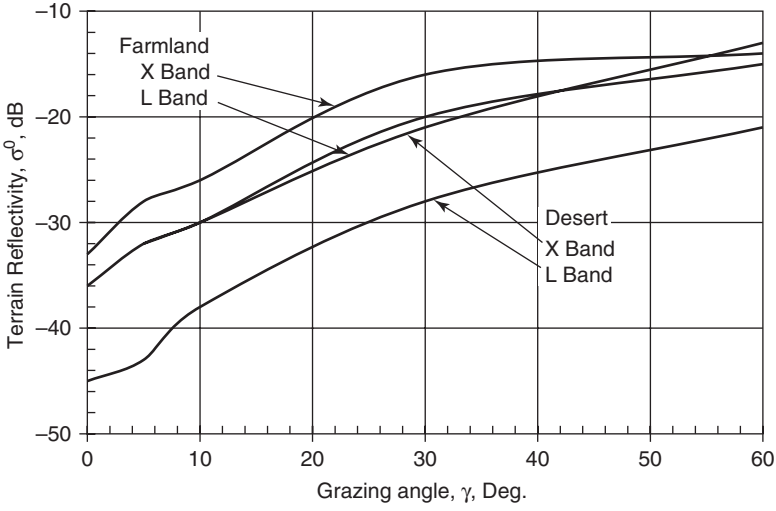

Fig. 4.12 Average terrain clutter reflectivity vs. grazing angle for L and X bands (data from [30])

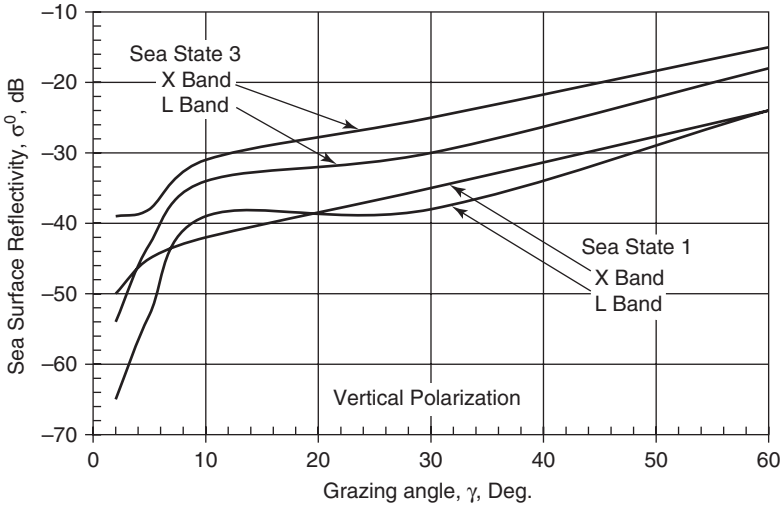

Fig. 4.13 Average sea clutter reflectivity vs. grazing angle for L and X bands (data from [30])

The volume of the clutter resolution cell, V_C, is:

$$V_C = \frac{\pi\ R^2\,\theta_A\,\theta_E\,\Delta R}{4} \tag{4.14}$$

where R is the target range, θ_A and θ_E are the azimuth and elevation beamwidths, ΔR is the range resolution. Equation 4.14 assumes that rain fills the radar resolution cell. When this is not so, the actual volume of rain in the resolution cell should be used.

Rain clutter reflectivity is characterized by a volume reflectivity parameter, η, which has the dimension m^{-1}, (square meters of clutter per cubic meter of rain), and is given by:

$$\eta = \frac{6 \times 10^{-14}\, r^{1.6}}{\lambda^4} \tag{4.15}$$

where r is the rainfall rate in mm/hr (Fig. 4.14). Equation 4.15 shows that rain clutter increases with rainfall rate and with the fourth power of frequency.

The clutter RCS in the resolution cell is given by:

$$\sigma_C = \frac{\eta\ V_C}{L_{BS}} \tag{4.16}$$

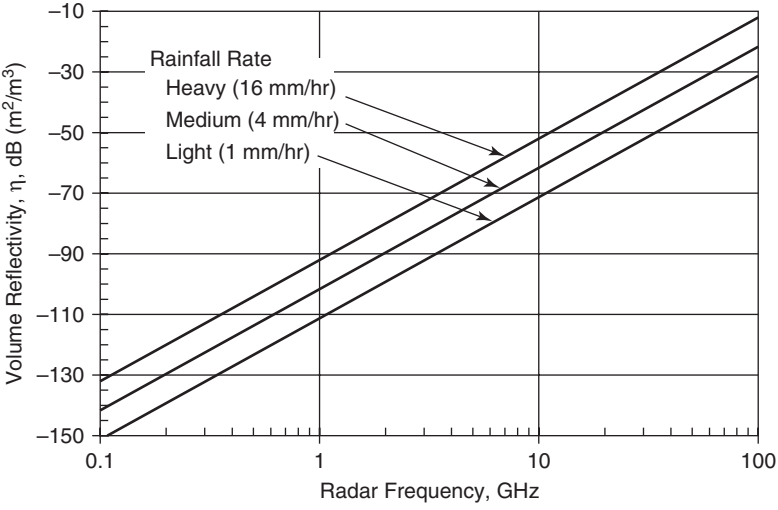

Fig. 4.14 Rain volume reflectivity vs. frequency and rainfall rate

where L_{BS} is a beam-shape loss for the clutter, equal to about 2.1 (3.2 dB). The signal-to-clutter ratio is:

$$\frac{S}{C} = \frac{\sigma \, \mathrm{CRL}_{BS}}{\eta \; V_C} \tag{4.17}$$

The S/C in rain (Eq. 4.17) varies inversely with η, and decreases with rainfall rate and radar frequency.

The velocity of rain clutter is generally that of the wind. Velocity spread is of the order of 2 to 4 m/s.

Clutter reduction. Since clutter results mainly from scatterers in the radar resolution cell, it is minimized by using small radar angle resolution (narrow beamwidth), and small range resolution (wide signal bandwidth). Other techniques for clutter reduction include:

- Moving-target indication (MTI), used by surface radars to cancel clutter (Sec. 5.2).
- Pulse-Doppler processing, used by airborne and space-based radars, as well as some surface radars to avoid and reject clutter (Sec. 5.3).
- Radars using circular polarization can reject rain clutter by receiving the same sense circular polarization transmitted. This rejects spherical raindrops, while having only a small effect on the signal from most complex targets (Sec. 3.1).

The ability of these techniques to reduce clutter depends on the clutter characteristics, radar stability and dynamic range, and details of clutter canceller design and associated signal processing. Typical cancellation ratios (CR) are in the 20–40 dB range.

4.6 Ionospheric Effects

The ionosphere comprises layers of ionized electrons at altitudes between about 55 and 1,000 km. Radar propagation paths that pass through the ionosphere can be affected. These paths include surface and airborne radars observing objects in space, and space-based radars observing terrestrial and airborne targets. The ionospheric effects on radar propagation vary inversely with various powers of radar frequency and are rarely significant at frequencies above about 1 GHz [33].

Ionospheric characteristics. Ionospheric effects on propagation depend on the integrated electron density along the signal path. For signal paths through the ionosphere, this decreases with increasing elevation angle. For paths ending in the ionosphere, it increases within range.

The electron density in the ionosphere is highly variable, and depends on:

- Solar radiation. It is significantly higher in the daytime than at night.
- Latitude. It is greatest at about 20 degrees latitude and in polar regions.
- Sunspot activity. It is higher in periods of increased sunspot activity.

This variability makes it difficult to predict the magnitude of ionospheric effects on radar propagation, and to correct for them.

Ionospheric attenuation. The attenuation from the ionosphere (in dB), varies inversely with the square of frequency. It is usually significant only at frequencies below about 300 MHz. The normal daytime two-way attenuation for signal paths passing through the ionosphere is shown vs. elevation angle for VHF and UHF frequencies in Fig. 4.15. At nighttime, the ionospheric attenuation is less than 0.1 dB for all elevation angles [33].

The non-uniform electron density in the ionosphere can produce random fluctuations in signal amplitude and phase in the VHF and UHF bands, and sometimes at L band. While these do not affect the average signal power, they can affect detection performance, especially when coherent integration is used (Sec. 3.3).

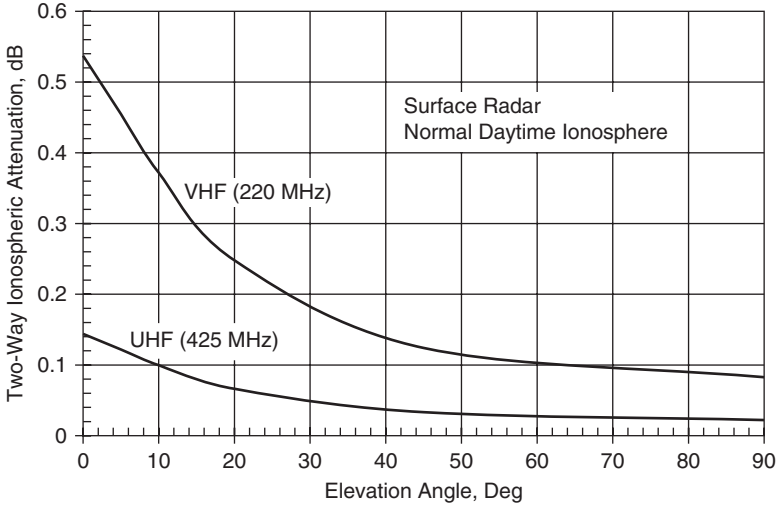

Fig. 4.15 Ionospheric attenuation at VHF and UHF frequencies vs. elevation angle for normal daytime ionospheric conditions (data from [33])

Ionospheric refraction. The refractive index in the ionosphere is less than unity, causing the signal path for a terrestrial radar to bend downward as it enters the ionosphere, and then upward as it leaves the ionosphere, so that is parallel with, but offset from, the signal path entering the ionosphere. This produces elevation-angle and range errors, which vary inversely with the square of frequency.

These errors are shown for a surface-based radar with a normal daytime ionosphere vs. range and elevation angle for VHF and UHF frequencies in Figs. 4.16 through 4.19 [33]. Nighttime errors are about one third of those plotted in the figures, while daytime errors during periods of ionosphere disturbance may be as much as three times those plotted. This wide range makes it difficult to correct for ionospheric refraction errors, unless the ionospheric conditions are measured.

Frequency dispersion. The variation of refractive index with frequency produces frequency dispersion of signals passing through the ionosphere. This limits the maximum signal bandwidth that can be supported by such signal paths. The maximum bandwidth varies as the 1.5 power of frequency.

Approximate values of maximum signal bandwidth for signals passing through the ionosphere are given vs. frequency and elevation angle

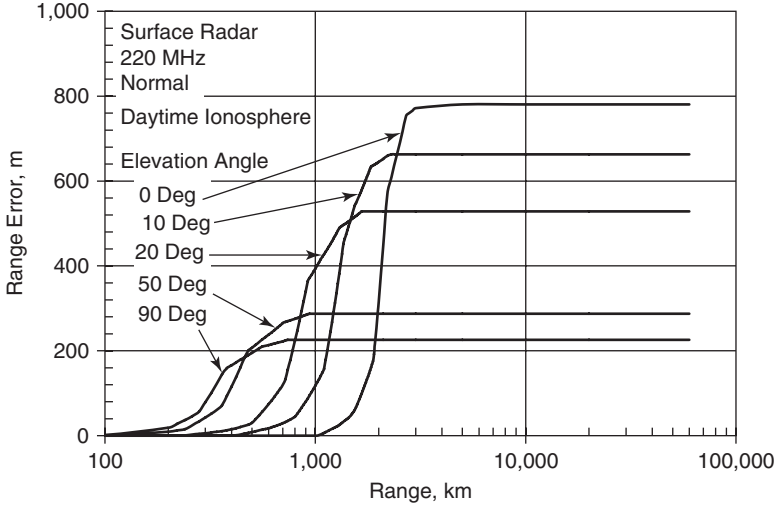

Fig. 4.16 Range errors at 220 MHz for normal daytime ionospheric conditions vs. range and elevation angle (made using the custom radar functions in [5])

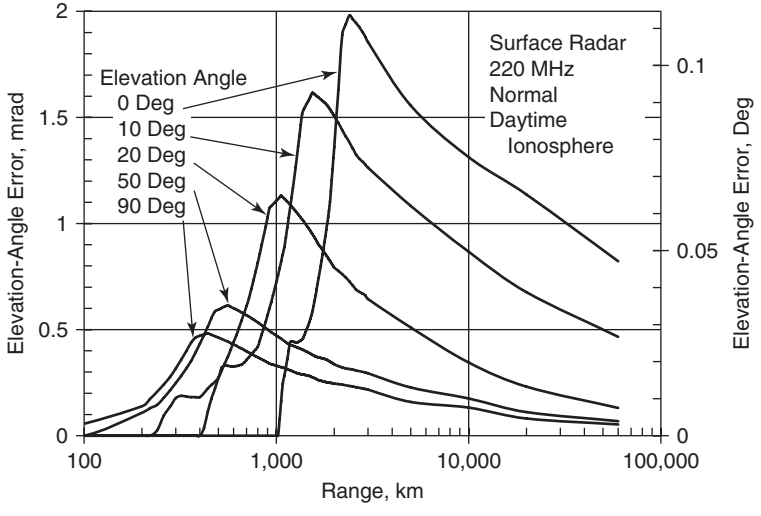

Fig. 4.17 Elevation-Angle errors at 220 MHz for normal daytime ionospheric conditions vs. range and elevation angle (made using the custom radar functions in [5])

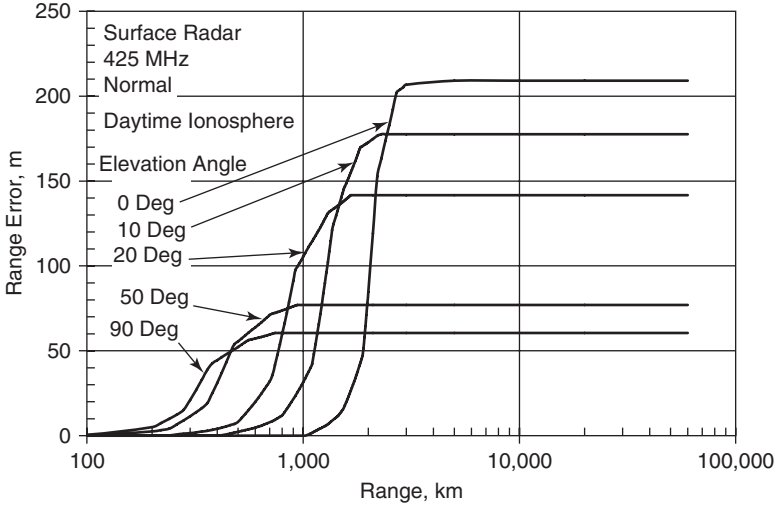

Fig. 4.18 Range errors at 425 MHz for normal daytime ionospheric conditions vs. range and elevation angle (made using the custom radar functions in [5])

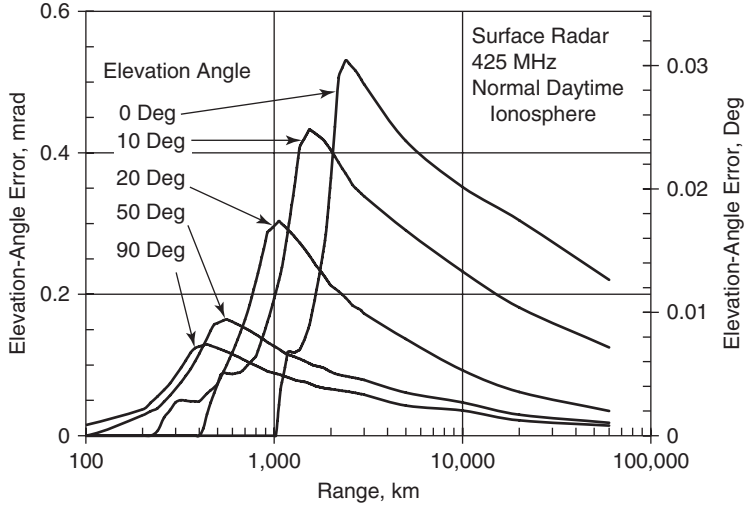

Fig. 4.19 Elevation-Angle errors at 425 MHz for normal daytime ionospheric conditions vs. range and elevation angle (made using the custom radar functions in [5])

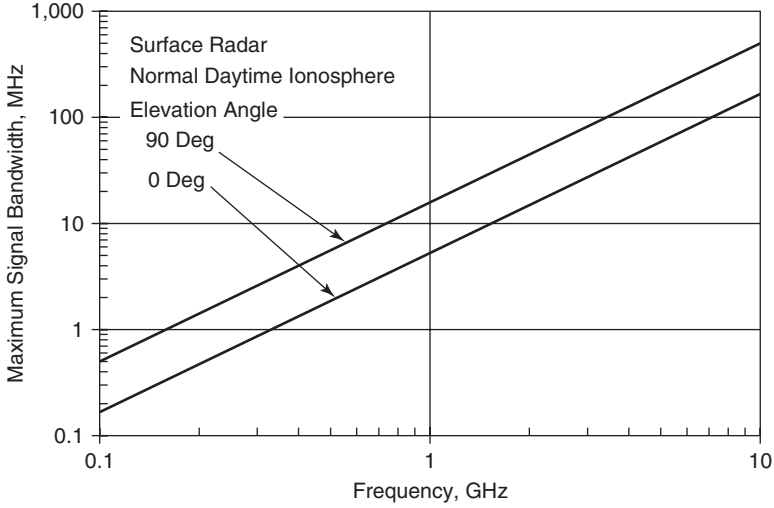

Fig. 4.20 Approximate maximum bandwidth for signals traversing the ionosphere vs. frequency and elevation angle for normal daytime ionosphere (data from [33])

for a normal daytime ionosphere in Fig. 4.20. Compensation for the estimated dispersion may allow larger bandwidths to be used. Nighttime bandwidths are significantly larger than in daytime.

Polarization rotation. The polarization of linearly-polarized signals rotates when passing through the ionosphere. The magnitude of this rotation is inversely proportional the square of frequency. At frequencies below about 2 GHz, the polarization of the received signal may not match that of the transmitted signal [33]. This could produce a significant signal loss unless dual linear polarizations are received. This condition may be mitigated by using circular polarization, which is not affected by ionospheric rotation.

4.7 Electronic Countermeasures (ECM)

Radars may be subject to deliberate electronic interference measures, termed electronic countermeasures (ECM). These can be categorized as (Table 4.2):

- Masking of radar targets, often using noise jamming or radar chaff.
- Confusion, by producing many false targets, often using pulse jamming or physical objects.

TABLE 4.2 Common Radar Countermeasures and Counter-Countermeasures (source: [5, Ch 10])

Category	Countermeasure	Counter-Countermeasures
Masking	Mainlobe jammer	Frequency agility
		Burnthrough
		Passive tracking
	Sidelobe jammer	Low sidelobes
		Frequency agility
		Burnthrough
		Sidelobe cancellers
	Volume chaff	MTI and pulse-Doppler
		Range resolution
		Velocity resolution
Confusion	Pulsed jammer	Sidelobe blanker
		Frequency agility
		Tracking
	Traffic decoys	Range resolution
		Bulk filtering
		Tracking
	Debris	Bulk filtering
		Tracking
Deception	Repeater jammer	Frequency agility
		PRF agility
		Signal processing
	Track-breaking jammer	Signal processing
		Tracking
	Spot chaff	MTI and pulse Doppler
		Radar measurements
		Tracking
	Decoy	Radar measurements
		Tracking

- Deception by creating false targets, either electronically or using decoy objects, or by breaking track on actual targets.

Radar designers and operators employ electronic counter-countermeasures (ECCM), to reduce the impacts of ECM on radar performance. These can include radar design features, operating modes, and dedicated ECCM techniques.

Common ECM techniques and potential ECCM responses are summarized below.

Noise jamming. Noise jammers attempt to mask radar targets by increasing the level of the noise competing with the target signal. Noise-jammer effectiveness is characterized by a signal-to-jammer power ratio, S/J. When the jammer noise has Gaussian probability density, S/J can be combined with S/N to give an overall signal-to-interference ratio:

$$\frac{S}{J+N} = \frac{1}{\frac{1}{S/J} + \frac{1}{S/N}} \tag{4.18}$$

Then $S/(J+N)$ can be used in place of S/N in calculating radar detection and measurement performance (Sec. 3.3 and 3.5). Radars often use constant-false-alarm-rate, (CFAR), techniques to automatically raise the detection threshold in the presence of jamming to maintain the false-alarm rate (Sec. 3.3).

A noise jammer can be described by its noise bandwidth, B_J, and its effective radiated power (ERP), which is the power density radiated in the direction of the radar to be jammed. The ERP is given by:

$$\text{ERP} = \frac{P_J G_J}{L_J} \tag{4.19}$$

where P_J is the jammer RF power, G_J is the jammer antenna gain in the direction of the radar, and L_J accounts for any jammer losses. ERP is often specified in dB relative to a Watt, dBW (Sec. 6.3).

Only the jammer noise power within the radar signal bandwidth, B, is effective in masking the target. However, if the jammer does not know the exact radar signal frequency, or if the radar changes its frequency from pulse to pulse (frequency agility), the jammer may have to jam a much wider bandwidth, B_J, to assure that the radar band is jammed. This is called barrage jamming.

Equation 4.19 assumes that the jammer polarization is aligned with that of the radar to be jammed. If the jammer does not know the radar polarization or can not control its orientation, two jammers with independent noise sources and orthogonal polarizations must be used. The ERP from Eq. 4.19 is then referred to as the ERP per polarization.

Jammer performance and radar ECCMs depend on whether the jammer is in the main radar beam or in a sidelobe region:

- Mainlobe jammers (MLJ). These signals enter the radar through the radar main radar beam. The jammers may be located on the

target itself and called self-screening jammers (SSJ), or they may be located on a vehicle near the target and called escort jammers (ESJ). The S/J for a MLJ is given by:

$$\frac{S}{J} = \frac{P_P\, G_T\, \sigma\, \mathrm{PC}\; B_J}{4\pi\; R^2\, BL_T\, \mathrm{ERP}} \tag{4.20}$$

where L_T is the radar transmit losses, and $B_J \geq B$. The S/J is determined by the signal reflected by the target and the jammer ERP, and is independent of receiver parameters. Like S/N, S/J can be increased by using pulse integration (Sec. 3.2). The range at which a target may be observed with a desired S/J is called the burnthrough range:

$$R = \left[\frac{P_P\, G_T\, \sigma\, \mathrm{PC}\; B_J}{4\pi\; (S/J)\; BL_J\, \mathrm{ERP}}\right]^{1/2} \tag{4.21}$$

Since MLJs are at or near the target, passively tracking them can reveal the target location.

- Sidelobe jammers (SLJ). These signals enter the radar through the radar sidelobes. The jammers are often deployed at long ranges, outside the coverage of hostile weapons. Then they are called stand-off jammers (SOJ). The S/J for a SLJ is given by:

$$\frac{S}{J} = \frac{P_P\, G_T\, \sigma\, \mathrm{PC}\;\; R_J^2\, B_J}{4\pi\; R^4\, B\; \mathrm{SL} L_T\, \mathrm{ERP}} \tag{4.22}$$

where R_J is the jammer range and SL is the radar sidelobe level at the jammer angle (a value less than unity, often represented by a negative dB value). Sidelobe jammers usually have higher power and gain than mainlobe jammers to overcome both the radar sidelobes and any increase in range. This requires that the jammer antenna be directed toward the targeted radar. The burnthrough range for SLJs is:

$$R = \left[\frac{P_P\, G_T\, \sigma\, \mathrm{PC}\, R_J^2\; B_J}{4\pi\; (S/J)\;\; B\;\; \mathrm{SL}\; L_J\, \mathrm{ERP}}\right]^{1/4} \tag{4.23}$$

Sidelobe cancellers (SLC) reduce the sidelobe level at the jammer angle. These use an auxiliary antenna to sense the jamming signal, adjust its amplitude and phase, and subtract it coherently from the main radar receive channel. Multiple SLCs can be used to cancel

multiple jammers. Phased array radars may calculate complex element weighting that minimizes the sidelobe levels at jammer angles. SLCs can reduce sidelobes by 20 dB or more.

Pulse jamming. Pulsed jammers produce false radar signals that confuse or deceive the radar operator or signal processor. Common techniques include:

- Sidelobe confusion jammers can produce large numbers of false targets in the radar sidelobe region and require radar and processing resources to confirm or reject them. Radars can reject sidelobe pulsed jammers by using sidelobe blankers (SLB). These use an auxiliary antenna to sense the timing of pulses entering the sidelobes, and blank the main receiver during these periods. These differ from the SLCs discussed above in that the radar is blanked during the pulse-arrival times. They can not be used with continuous jammers or the radar would be inoperative.
- Swept-spot jammers can create false targets as the jammer sweeps through the radar signal band. By using very-rapid sweep rates they can produce an effect similar to broadband noise and mask targets over the radar band.
- Repeater jammers transmit replicas of the radar signal to create false targets. These may be synchronized with the radar pulse transmissions to generate stationary targets or those on credible paths. If the radar frequency changes, the repeater frequency must follow those changes. This limits the false-target positions to ranges greater than that of the jammer, which is often located on a real target.
- Track-breaking jammers are usually located on a target that is being tracked by the radar. They emit sophisticated signals timed and phased to move the range or angle tracking gates off the real target so that track is lost.

Sidelobe blanking, frequency agility and PRF changes reduce the effectiveness of many pulsed jamming techniques. Radar signal and data processors are sized to handle the remaining target load.

Volume chaff. Radar volume chaff consists of a large number of small scatterers located around a target of interest. The reflections from the chaff are intended to mask the radar signal return from the target. Chaff may be deployed in a cloud around a target, or in a corridor to mask targets that pass through.

Chaff effectiveness is characterized by a signal-to-chaff RCS ratio, S/C. When the chaff return has Gaussian probability density, S/C can be combined with S/N to give an overall signal-to-interference ratio:

$$\frac{S}{C+N} = \frac{1}{\frac{1}{S/C} + \frac{1}{S/N}} \tag{4.24}$$

Then $S/(C+N)$ can be used in place of S/N in calculating radar detection and measurement performance (Sec. 3.3 and 3.5).

Dipoles that are resonant at the radar frequency are often used for chaff. They have a length of $\lambda/2$ and an RCS average over all angles of $0.15\lambda^2$ [20]. The total RCS, σ_C, for n_C dipoles is:

$$\sigma_C = 0.15\, n_C\, \lambda^2 \tag{4.25}$$

The total chaff RCS can be empirically related to the chaff weight. For common chaff technology [6, Ch. 3]

$$\sigma_C \approx 22,000\ \lambda\ W_C \tag{4.26}$$

where W_C is the total chaff weight in kg. Note that the overhead weight for deploying chaff often equals the chaff weight itself.

Dipole chaff covers a signal bandwidth of about 10%. For larger bandwidths, or to cover multiple radar bands, multiple chaff lengths are used.

In most cases, chaff that interferes with the target is in the same range-angle resolution cell as the target. The volume of the chaff resolution cell, V_C, is:

$$V_C = \frac{\pi\ R^2\, \theta_A\, \theta_E\, \Delta R}{4} \tag{4.27}$$

where R is the target range, θ_A and θ_E are the azimuth and elevation beamwidths, ΔR is the range resolution. Equation 4.27 assumes that chaff fills the radar resolution cell. When this is not so, the actual volume of chaff in the resolution cell should be used.

If the chaff is uniformly distributed over a volume, V_T, then the chaff RCS in the resolution cell that interferes with the target, C, is:

$$C = \frac{\sigma_C\, V_C}{V_T\, L_{BS}} \tag{4.28}$$

where L_{BS} is a beam-shape loss for the chaff, equal to about 2.1, (3.2 dB). The signal-to-chaff ratio is:

$$\frac{S}{C} = \frac{\sigma\, V_T\, L_{BS}\, CR}{\sigma_C\, V_C} \tag{4.29}$$

where CR is a chaff cancellation ratio. Since chaff is usually not uniformly distributed, Equations 4.28 and 4.29 should be considered as approximate.

Chaff deployed in the atmosphere quickly slows to the air speed, while airborne targets usually have much larger velocity. MTI (Sec. 5.2), or pulse-Doppler processing (Sec. 5.3), can provide chaff cancellation of the order of 20–40 dB. Exoatmospheric chaff has a velocity spread produced by its dispensing mechanism, and waveforms having good radial-velocity resolution (Sec. 5.1), may provide useful chaff cancellation.

Objects. Physical objects may be used to confuse or deceive radar operations. These can include:

- Traffic decoys, small objects having observables roughly similar to the targets to be protected. The objective is to overload the radar processor. A radar may use simple thresholds or bulk-filtering techniques such as RCS, or RCS fluctuation rate to reject these.
- Debris from rocket or missile stages and deployment mechanisms may have effects similar to that of deliberate traffic decoys.
- Spot chaff, small clusters of chaff particles, may create false targets. These may be rejected based of radar observables or velocity in the atmosphere.
- Replica decoys are objects designed to match a target's radar observables, and often travel on credible flight paths. Techniques for discriminating between these and actual targets are discussed in Sec. 5.5.